BIOCHEMISTRY
including biophysical chemistry & molecular biology
Article

Biochemistry **2010,** *49,* 3919–3927 3919
DOI: 10.1021/bi1002663

Antiparallel Dimer and Actin Assembly†

Elena E. Grintsevich,‡,∥ Martin Phillips,‡ Dmitry Pavlov,‡ Mai Phan,‡ Emil Reisler,‡ and Andras Muhlrad*,§,∥

‡*Department of Chemistry and Biochemistry and Molecular Biology Institute, University of California, Los Angeles, California 90095, and* §*Institute of Dental Sciences, School of Dental Medicine, The Hebrew University, Jerusalem 91120, Israel* ∥*These authors contributed equally to this work.*

Received February 22, 2010; Revised Manuscript Received March 31, 2010

ABSTRACT: The antiparallel dimer (APD) is a unique actin species, which can be detected in the early stages of actin polymerization. In this work, we introduce novel tools for examination of the effects of the APD on actin polymerization. We document that bifunctional methanothiosulfonate (MTS) reagents are an attractive alternative to the routinely used *p*-phenylene maleimide (pPDM) for APD detection, allowing for fast and efficient cross-linking under conditions of actin polymerization at neutral pH. We report also that pyrene-labeled yeast actin mutant A167C/C374A (C167PM) forms significant amounts of stable APD in solution, without chemical cross-linking or polymerization-affecting compounds, and that the kinetics of APD transformation and decay upon actin polymerization can be easily monitored. The dimerization of C167PM has been characterized in sedimentation equilibrium experiments ($K_d \sim 0.3\ \mu M$). This new system offers the advantage of assessing the effects of the APD under physiological conditions (pH, ionic strength, and Mg^{2+} concentration) and testing for conformational transitions in the APD during nucleation−polymerization reactions or/and in the presence of actin-interacting factors. The results obtained using two different systems (C167PM actin and polylysine-induced polymerization of α-actin) show that the APD decays at a rate slower than that at which the filaments elongate, revealing its transient incorporation into filaments, and confirm that it inhibits the nucleation and elongation of actin filaments.

The antiparallel dimer (APD)[1] is a unique actin species, which can be detected in the early stages of actin polymerization. Several techniques, such as chemical cross-linking (*1*), EM (*2*, *3*), and fluorescence spectroscopy (*4*), have been used to assess the role of APD in filament formation. As revealed by these methods, only small amounts of a fast-decaying APD form under conditions close to physiological, impeding its studies.

To stabilize the APD in solution, chemical cross-linking with pPDM and glutaraldehyde was employed in prior work (*1*, *3*). However, the pH switch required for the pPDM reaction and a low specificity of glutaraldehyde cross-linking complicate the interpretation of these results. It is not clear whether the amounts of the APD in the actin preparations are the same at pH 9.2 (pPDM cross-linking conditions) and pH 7−8 (actin polymerization conditions). Also, it should be noted that the dynamic properties of such cross-linked actin dimers must be different from those of the un-cross-linked APD. Nevertheless, several interesting observations were made using the cross-linking approach. It was documented that pPDM-cross-linked APD could neither nucleate actin assembly nor form filaments (*1*). A recent EM study of salt-induced actin polymerization supported this result and led to the conclusion that the APD contributed to the initial disordering of newly formed filaments rather than to their nucleation (*3*). It was also suggested on the basis of the results obtained with the cross-linked dimer that the ADP incorporated transiently into growing filaments, perhaps facilitating their branching (*2*). However, these findings are lacking direct kinetic evidence, which can be obtained only with the un-cross-linked APD.

The use of model polycations represents another approach to the APD studies (*4*, *5*). The formation of significant amounts of the APD in the presence of polylysine is particularly interesting because polyamine polycations spermine and spermidine (*6*, *7*), which are present in proliferating cells (at millimolar concentrations) (*8*, *9*), as well as polycationic proteins such as myelin basic protein (*10*), calponin (*11*), fesselin (*12*), lysozyme (*13*), and MARCKS (*14*) may induce the formation of the APD in vivo. Unfortunately, neither the formation nor the amount of the APD formed in the polylysine-induced actin polymerization could be quantified without actin cross-linking. However, a combination of polylysine and latrunculin A has been used successfully to obtain a homogeneous population of nonpolymerizable APD, which was suitable for crystallization (*4*).

The attention to APD's role in actin assembly was redrawn by Bubb et al. (*4*) after observation of the interaction between two APDs in a crystal structure. These authors proposed a model for filament nucleation by a complex of two APDs, involving a conformational transition to allow for filament growth (*4*). None of the approaches described above could be used to test this hypothesis: chemical cross-linking would not allow for the predicted conformational transition in the nuclei, and the polylysine-induced polymerization is too fast for nucleation studies.

†This work was supported by grants from U.S. Public Health Service (GM 077190) and the National Science Foundation (MCB 0316269) to E.R.

*To whom correspondence should be addressed. E-mail: muhlrad@cc.huji.ac.il. Phone: 972-2-6757587. Fax: 972-2-6758561.

[1]Abbreviations: APD, antiparallel dimer; C167, yeast actin mutant A167C/C374A; C167PM, yeast actin mutant A167C/C374A labeled with pyrene maleimide; MTS, methanothiosulfonate reagents; pPDM, *p*-phenylene maleimide.

Published on Web 04/02/2010

In this work, we introduced a novel tool for examining the effect of the APD on actin polymerization, which did not involve covalent cross-linking or the use of polycations. We showed that pyrene labeling of yeast actin mutant A167C/C374A (C167) led to the formation of a stable APD under nonpolymerizing conditions. Self-association of the pyrene-labeled C167 actin (C167PM) was characterized in equilibrium sedimentation experiments, and a K_d of 0.34 μM was determined. We also used a bifunctional disulfide reagent, 1,1-methanediyl bismethanethiosulfonate (MTS-1), which allowed for efficient and rapid actin cross-linking under conditions of polymerization reactions for monitoring the changes in the relative amounts of the APD in solution. Our results show that the APD inhibits actin filament nucleation and elongation, is incorporated transiently into growing filaments during the polymerization reaction, and persists at a lower level in the polycation-induced actin bundles.

MATERIALS AND METHODS

Reagents. *N*-(1-Pyrene)maleimide was obtained from Molecular Probes (Eugene, OR) or AnaSpec Inc. (San Jose, CA). Acrylodan and fluorescein maleimide (FM) were purchased from Molecular Probes. ATP, poly-L-lysine (MW 4000), dithiotreitol (DTT), *N*-ethylmaleimide (NEM), spermine, and EGTA were purchased from Sigma Chemical Co. (St. Louis, MO). 1,1-Methanediyl bismethanethiosulfonate (MTS-1), 1,3-propanediyl bismethanethiosulfonate (MTS-3), and 1,6 hexanediyl bismethanethiosulfonate (MTS-6) were obtained from Toronto Research Chemicals Inc. (North York, ON).

Proteins. CaATP-G-actin was prepared by the method of Spudich and Watt (*15*). MgATP-G-actin was obtained by incubating CaATP-G-actin with 0.2 mM EGTA and 0.1 mM $MgCl_2$ at room temperature for 5 min. MgATP-G-actin was diluted for further treatments in a buffer containing 5.0 mM Tris-HCl, 0.1 mM $MgCl_2$, 0.2 mM EGTA, 0.2 mM ATP, and 0.5 mM DTT (pH 8.0). MgATP-G-actin was used within 2 h following the preparation. The concentration of unlabeled skeletal muscle α-G-actin was determined spectrophotometrically using an extinction coefficient ($E^{1\%}_{290}$) of 11.5 cm^{-1}. Yeast actin mutant C167 was purified as described previously (*16*). Lysozyme was purchased from Sigma Chemical Co.

Chemical Modification. Labeling of skeletal F-actin at Cys-374 with pyrene maleimide was carried out according to the method of Kouyama and Mihashi (*17*) with some modifications. CaATP-G-actin was filtered through a PD-10 column equilibrated with a buffer containing 5.0 mM Tris-HCl, 0.2 mM $CaCl_2$, and 0.2 mM ATP (pH 8.0) (G buffer). After filtration, actin (1.0 mg/mL) was polymerized by 2.0 mM $MgCl_2$ and 100 mM KCl at room temperature for 30 min and reacted with pyrene maleimide at a 2-fold molar excess over actin, on ice, for 1 h. The reaction was terminated with 1.0 mM DTT. The labeled F-actin was centrifuged at 38K rpm, in a Ti 50 rotor, in a Beckman ultracentrifuge for 2 h, and then the pellet was resuspended in G buffer and depolymerized for more than 36 h at 4 °C. After dialysis, actin was centrifuged at 38K rpm for 2 h. The supernatant contained the purified pyrene-labeled CaATP-G-actin. The concentration of modified actin was determined by the procedure of Bradford (*18*) using unmodified actin as a standard. The extent of labeling, which was measured by using a pyrene extinction coefficient (E_{344}) of 22 mM^{-1}, was ~100%.

Labeling of C167 on G-actin was carried out in a buffer containing 5.0 mM Tris (pH 8.0), 0.2 mM $CaCl_2$, and 0.3 mM ATP. A 1.5-fold molar excess of PM or FM over actin was used in the modifications. Reaction mixtures were incubated on ice for 1 h or overnight. The labeling was stopped with 1.0 mM DTT. All samples were dialyzed overnight against buffer A [5.0 mM HEPES (pH 7.5), 0.2 mM $CaCl_2$, 0.2 mM ATP, 1.0 mM DTT, and 50 mM KCl]. The modified C167PM actin was filtered through a 0.22 μm filter. The extent of C167 actin labeling was assessed under denaturing conditions, in 5.3 M urea buffer (U buffer) using an ε of 20350 M^{-1} cm^{-1} for pyrene maleimide, which was determined as follows. The absorbance of pyrene maleimide was measured first in methanol (ε = 40000 M^{-1} cm^{-1}, λ_{max} = 338 nm) (Molecular Probes, The Handbook) and then in U buffer (λ_{max} = 343 nm). The absorbance ratio [A_{max}(methanol)/A_{max}(U buffer) = 1.96] was used to correct the PM extinction coefficient determined in methanol for U buffer conditions (40000 M^{-1} cm^{-1}/1.96 = 20350 M^{-1} cm^{-1}). The extinction coefficient of FM in U buffer was estimated by the same method using borate buffer (pH 9.0) instead of methanol (Molecular Probes, The Handbook). The yeast actin concentration was measured by the Bradford assay (*18*).

Covalent Cross-Linking. Cross-linking of two actin monomers between Cys-374 residues at the C-terminus was conducted with the MTS-1 disulfide reagent unless stated otherwise. Immediately prior to the cross-linking reaction, dithiothreitol was removed from CaATP-G-actin over a PD-10 column equilibrated with G buffer. Unless stated otherwise, MTS-1 was added to actin monomers at a 0.75:1.0 molar ratio immediately before the addition of polylysine. The cross-linking reaction was stopped with 1.0 mM NEM, 30−60 s after the addition of MTS-1. Cross-linked samples were analyzed via SDS−PAGE.

Fluorescence and Light Scattering Measurements. The time course of pyrene-labeled α-actin polymerization was monitored by the fluorescence increase (365 nm excitation and 386 nm emission) in a PTI spectrofluorometer (Photon Technology Industries, South Brunswick, NJ). The time course of excimer formation during actin polymerization was followed with 343 nm excitation and 478 nm emission wavelengths either in a PTI spectrofluorometer or in an Applied Photophysics (Leatherhead, Surrey, U.K.) stopped-flow apparatus supplied with excitation and emission monochromators. Light scattering was also measured in a PTI spectrofluorometer with both excitation and emission wavelengths set at 450 nm. The polymerization of C167PM was monitored by the fluorescence increase (344 nm excitation and 396 nm emission). Phalloidin-stabilized F-actin seeds were obtained as described previously (*19*).

Analytical Centrifugation. For sedimentation equilibrium experiments, 167PM actin (4, 12, and 20 μM, 100% labeled) was centrifuged in a 12 mm six-sector cell in a Beckman XLA analytical ultracentrifuge at 9000, 10500, and 12500 rpm in buffer A, at 20 °C. Absorbance scans at 290 nm were made at each speed after allowing at least 28 h for equilibrium to be obtained. Buffer density was 1.001. A partial specific volume of 0.735 mL/g for the complex was calculated from the amino acid composition of yeast actin, corrected to 20 °C (*20*, *21*). The "multifit" option of the Beckman Origin-based software (version 3.01) was used to analyze the nine scans, corresponding to the three input concentrations and the three speeds, simultaneously, for various monomer−multimer models. The best fit was obtained with a monomer−dimer model.

For sedimentation velocity, 400 μL samples (30 μM, 72% labeled) were loaded into double-sector cells at 20 °C. Absorbance scans were made at 4 min intervals at 343 nm [λ_{max}(pyrene maleimide)]. Sedimentation coefficients were determined from

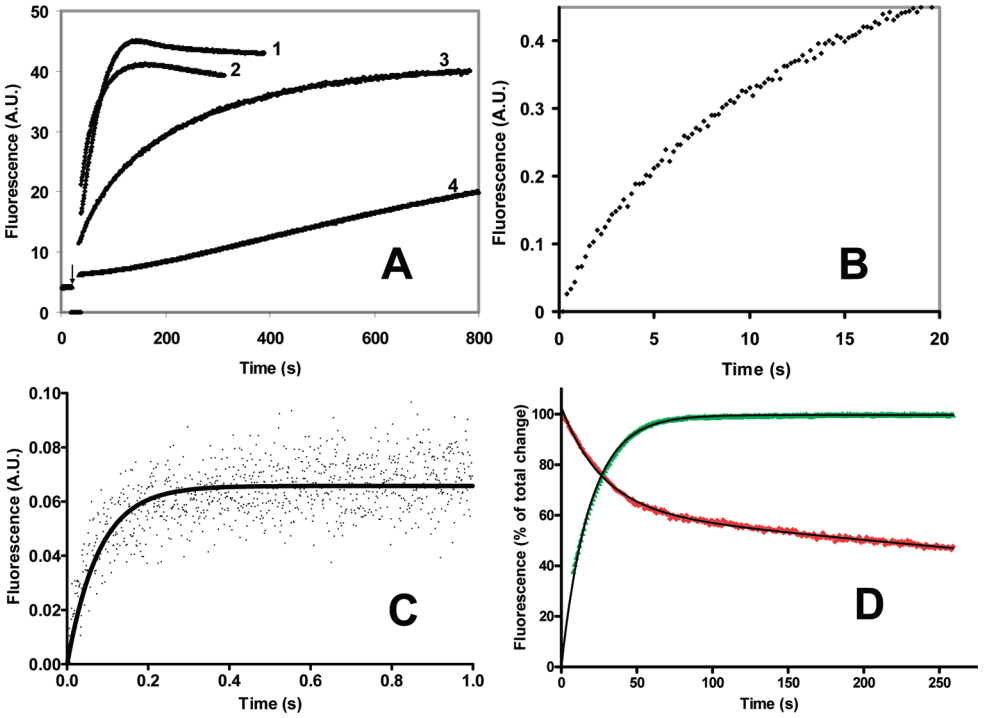

FIGURE 1: (A) Polymerization of 1.5 μM pyrene-labeled (100%) skeletal Mg-ATP-G-actin [5 mM Tris (pH 8), 0.1 mM $MgCl_2$, 0.2 mM EGTA, 0.2 mM ATP, and 0.5 mM DTT] with (1) 4.0 μM polylysine containing 0.2 mM $MgCl_2$, (2) 4.0 μM lysozyme, (3) 0.5 mM spermine, or (4) 2.0 mM $MgCl_2$. The polymerization was followed in a PTI spectrofluorometer (see Materials and Methods). (B) Actin polymerization of 2.0 μM pyrene-labeled Mg-ATP-G-actin by 4.0 μM polylysine and 0.2 mM $MgCl_2$ at pH 8 (G buffer) followed in a stopped-flow fluorometer (see Materials and Methods). (C) Excimer formation during the polymerization of 2.0 μM pyrene-labeled (100%) Mg-ATP-G-actin by 4 μM polylysine and 0.15 mM $MgCl_2$ at pH 8.0 followed in a stopped-flow fluorometer (see Materials and Methods). (D) Kinetics of actin filament elongation (green) and excimer fluorescence decay (red). Polylysine (4.0 μM) and $MgCl_2$ (0.1 mM) were added to 1.5 μM pyrene-labeled (100%) MgATP-G-actin. Excimer fluorescence decay started 9 s after polylysine addition but was shifted to 0 s in this figure. The elongation and excimer decay data were fitted to single- and two-exponential equations (black lines) with rate constants of 0.054 s^{-1} for elongation and 0.037 and 0.0005 s^{-1} for excimer decay. The change in fluorescence is shown as a percentage of the total change upon elongation (365 nm excitation and 386 nm emission) and excimer decay (343 nm excitation and 478 nm emission).

the peaks of $g(s)$ plots of the sedimentation coefficient distribution, determined using the Beckman Origin-based software (version 3.01). The sedimentation coefficient for the C167 dimer was estimated from the concentrations of the monomer and dimer. These concentrations were determined from the equilibrium constant measured by sedimentation equilibrium and the input concentration (30 μM 167PM, 72% labeled), a value of 3.25 S for monomeric yeast actin, and the measured weight-average sedimentation coefficients.

Electron Microscopy. Actin samples were applied to 400-mesh carbon-coated copper grids coated with Formvar films (EM Sciences) and stained with 1% uranyl acetate. The grids were examined with a Tecnai TF20 electron microscope (FEI) operated at 80 kV.

RESULTS

Polylysine-Induced Actin Polymerization and Formation of the APD. The polymerization of 1.5 μM pyrene-labeled MgATP-G-actin can be induced by natural polycations such as lysozyme and spermine, as well as by the model compound polylysine (Figure 1A). To optimize such a polymerization reaction, a low concentration of $MgCl_2$ (0.2 mM), which did not polymerize actin alone, was added together with polylysine. The polycation-induced polymerization of MgATP-G-actin was very fast in the presence of polylysine and lysozyme (at micromolar concentrations) and somewhat slower with spermine (0.5 mM). In contrast to the Mg^{2+}-stimulated reaction, the polylysine-induced polymerization proceeded without any observed lag phase (Figure 1A), which was confirmed also in a stopped-flow experiment (Figure 1B). The lag phase was absent even at low actin concentrations [0.1−0.4 μM (data not shown)]. Thus, the critical concentration for polycation-induced polymerization is much lower than that for the Mg-mediated actin polymerization (0.1 μM MgATP-G-actin was not polymerized by 2.0 mM $MgCl_2$ under our experimental conditions).

It was previously shown via excimer fluorescence from pyrene-labeled actin that the onset of a polycation-induced actin polymerization was accompanied by formation of the APD in amounts much greater than those noted during a divalent cation-induced polymerization (*4*). We observed a similar effect of polylysine on pyrene excimer formation during actin polymerization, while no excimer was detected when Mg-ATP-G-actin was polymerized at the same concentration (1.5 μM) with 2.0 mM $MgCl_2$ (data not shown). Initial excimer formation in the polylysine-induced actin polymerization was very fast (Figure 1C), and it was followed by a biphasic (fast and then slow) excimer decay (Figure 1D). The pre-steady state kinetics of excimer formation was monitored in a stopped-flow spectrofluorometer. The data were fitted to a single-exponential equation with a rate constant of 12.8 ± 0.5 s^{-1}, reaching a plateau within ~0.2 s of the addition of polylysine (Figure 1 C). We also found that the decay of excimer fluorescence started 8−9 s after the addition of polylysine, when ~40% of the actin was already polymerized.

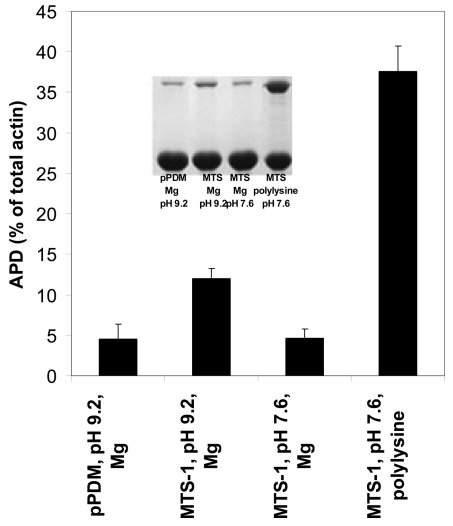

FIGURE 2: Assessing relative amounts of the APD by MTS and pPDM cross-linking. MgATP-G-actin (9.0 μM) was cross-linked by 4.5 μM pPDM or 6.0 μM MTS-1 during its polymerization by 2.0 mM $MgCl_2$ or 16 μM polylysine at pH 9.2 or 7.6. $MgCl_2$ and pPDM or MTS-1 were added together to MgATP-G-actin in the presence of 6.0 mM borate buffer (pH 9.2) or 5.0 mM MOPS buffer (pH 7.6); the cross-linking reaction was quenched with 1 mM NEM after 1 min. In the polylysine-induced polymerizations, MTS-1 was added first and was followed immediately by the polylysine. Reactions were quenched with 1.0 mM NEM 30 s after their onset. Products of reactions were analyzed by SDS−PAGE. Error bars correspond to mean errors of three independent experiments.

Assessing Relative Amounts of the APD by Chemical Cross-Linking. Although the rates of APD formation could be monitored via its excimer band, this method does not determine the amount of dimer present in the polymerization reaction mixture. Previously, 1,4-PDM (pPDM) and glutaraldehyde cross-linking of actin were used for that purpose (*1*). However, such cross-linking reactions do not measure equilibrium concentrations of the APD. Moreover, the low specificity of glutaraldehyde and a pH shift (from pH 7.5−8 to 9.2) needed to conduct pPDM cross-linking may complicate the interpretation of results.

To improve on the assessment of the APD presence under conditions of actin polymerization (pH 7.0−8), we employed the bismethanethiosulfonate (MTS) cross-linking reagents. These bifunctional reagents react with sulfhydryl groups fast and efficiently at neutral pH. Three MTS with increasing cross-linking spans, MTS-1, MTS-3, and MTS-6, were tested for APD cross-linking. All of them produced similar amounts of the APD in test reactions (2.0 μM MgATP-G-actin polymerized by 4.0 μM polylysine and 0.2 mM $MgCl_2$) and yielded no dimer under nonpolymerizing conditions (data not shown). Thus, in all subsequent cross-linking experiments, we used MTS-1 (at an optimal mole ratio to actin of 0.75:1), which spans the shortest cross-linking distance (5.4 Å) that is consistent with the crystal structure of the APD (*4*). A comparison of actin cross-linking by MTS-1 and pPDM during Mg-induced polymerization at pH 9.2 revealed a more efficient reaction with MTS-1, yielding more APD under identical reaction conditions (Figure 2). As expected, the yield of APD was much higher in the polylysine-induced than in the Mg-induced polymerization (Figure 2). MTS-1 cross-linking captured also more APD at pH 9.2 than at pH 7.6. These data show efficient capturing of the APD species via MTS reaction and a potential complication associated with a pH shift involved in pPDM cross-linking.

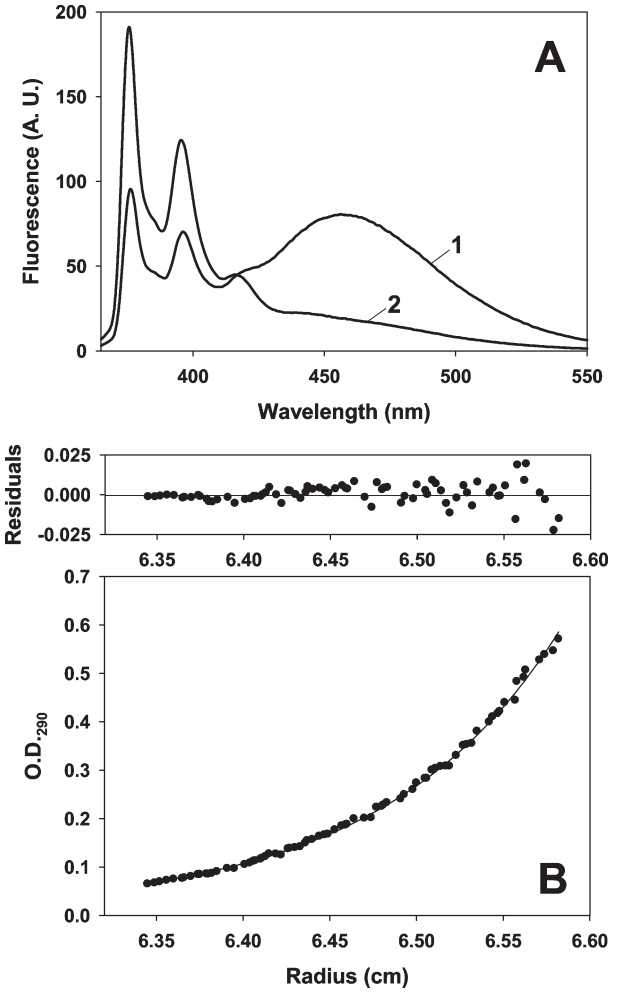

FIGURE 3: (A) Excimer formation in the preparation of pyrene maleimide-labeled actin mutant C167 (20 μM, C167PM) (1). A characteristic excimer peak disappears upon actin polymerization (2). Conditions: 5.0 mM HEPES (pH 7.5), 0.2 mM $CaCl_2$, 0.2 mM ATP, 1.0 mM DTT, and 50 mM KCl (buffer A). Actin polymerization was induced by 3.0 mM $MgCl_2$. (B) Sedimentation equilibrium of C167PM (12 μM, 100% labeled). The solid curve shows the best fit to the data assuming a monomer−dimer equilibrium with a K_d of 0.34 μM. The top panel shows the distribution of residuals relative to the theoretical curve. Sedimentation experiments were performed in buffer A at 20 °C. Protein absorbance was measured at 290 nm.

Pyrene-Labeled Yeast Actin A167C/C374A: A New System for Studying the APD. Yeast actin mutant A167C/C374A (C167), which has only one reactive cysteine at position 167, shows normal polymerization properties and a nucleotide exchange rate identical to that of wild-type (WT) yeast actin (Kudryashov et al., manuscript to be published). The labeling of C167 with pyrene maleimide leads to the formation of protein species with a characteristic excimer peak ($\lambda_{max} \sim 455$ nm), which disappears upon actin polymerization (Figure 3A). Under nonpolymerizing conditions [5.0 mM HEPES G buffer (pH 7.5)], these species are stable for several days. Addition of monovalent salt, up to 100 mM KCl, leads to a slight increase in the magnitude of the excimer signal without actin polymerization. As described previously (*22*), excimer formation requires the overlapping and stacking of pyrene rings and sets the limit of maximum 18 Å separation between pyrene-modified cysteines in protein complexes or within the same molecule. According to a previously published crystal structure of the APD [Protein Data Bank (PDB) entry 1LCU] (*4*), the Cα−Cα distance between the

two residues at position 167 in this dimer is ~14.6 Å, which satisfies the condition for pyrene excimer formation (Figure S1 of the Supporting Information) (*22*). PAGE under native conditions confirmed the presence of the actin dimer in solution: only two bands corresponding to the actin monomer and actin dimer were detected (data not shown), indicating that the observed formation of the excimer is not due to nonspecific actin aggregation.

To characterize the C167PM self-association more accurately, sedimentation equilibrium experiments were performed on samples of 100% labeled C167PM actin (4, 12, and 20 μM; see Materials and Methods and Figure 3B for details). The resulting data could be fitted well to a monomer−dimer equilibrium system. Alternative equilibrium models (monomer−trimer and monomer−dimer−trimer) did not yield good data fits. On the basis of the sedimentation equilibrium experiments, the K_d (dimerization constant) of the C167PM APD was estimated to be ~0.34 μM. Sedimentation velocity experiments confirmed the monomer−dimer equilibrium, allowing for a calculation of the dimer sedimentation coefficient from the observed sedimentation coefficient, the sedimentation coefficient of the actin monomer (3.25 S), and the K_d determined above. The calculated value (S_{dimer} = 4.64 S) is close to the coefficient previously determined for the APD in the presence of polylysine and latrunculin A (4.8 S) (*4*). Thus, we documented and characterized quantitatively the formation of a stable APD in pyrene-labeled C167 actin preparations. We use this new system as a tool to study the role of the APD in actin polymerization.

The APD Inhibits Actin Nucleation. The polymerization of 100% labeled C167PM actin (15 μM) by 3.0 mM $MgCl_2$ is shown in Figure 4A. Considering K_d ~ 0.3 μM, most of the pyrene-labeled C167 actin in this sample should be in the APD form under nonpolymerizing conditions. No polymerization of this actin was detected more than 30 min after the addition of Mg^{2+}, but the polymerization could be rescued to some extent with phalloidin-stabilized actin seeds (Figure 4A). Despite unconventional polymerization kinetics [without reaching a plateau within several hours (Figure 4A)], the EM analysis of these samples (after overnight incubation on ice) revealed the presence of actin bundles consisting of regular filaments (Figure 4A, inset). The polymerization of the pyrene-labeled C167 actin mutant could be rescued more efficiently with the addition of equimolar concentrations of phalloidin (Figure 4B). However, loose actin bundles were observed by EM in these samples (Figure 4B, inset). These observations suggested that not only the nucleation but also initial stages of filament formation and/or filament elongation were affected by the APD.

To ensure that the observed effects are not caused by mere labeling of C167 on actin, this residue was modified with two other probes (fluoresceine maleimide and acrylodan) and compared to C167PM under identical polymerization conditions. As shown in Figure 5, the polymerization of C167PM actin (12 μM, 69% labeled) was much slower than that of C167 (12 μM) labeled to the same extent with fluoresceine maleimide (FM), which exceeds in size the pyrene probe (*23*). Also, C167PM actin, but not C167FM, showed a lag phase in the assembly reaction (Figure 5, inset). A comparison of the C167PM and acrylodan-modified C167 actins revealed similar effects (data not shown). These results confirm that actin nucleation is inhibited by the APD and not the labeling of Cys-167 on actin.

The APD Is Incorporated into the Actin Filament and Inhibits Its Elongation. To test whether the APD could be incorporated into actin filaments, we used the fact that the pyrene fluorescence of C167PM actin (at λ values of 375 and 396 nm) increases upon its polymerization. Thus, we monitored simultaneously the C167PM actin polymerization (λ = 396 nm) and

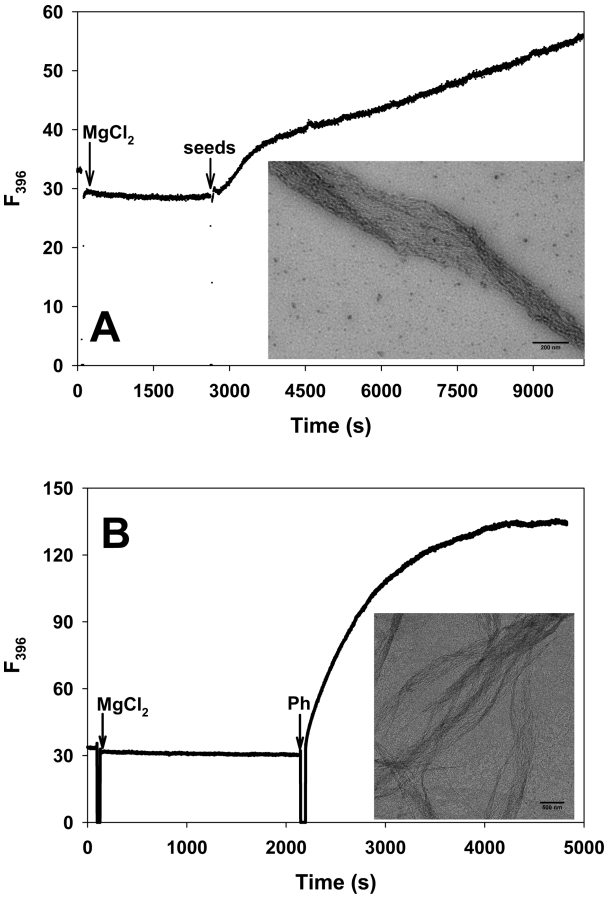

FIGURE 4: (A) Polymerization of C167PM (15 μM, 100% labeled) actin in the presence of 3.0 mM $MgCl_2$, rescued by the addition of 50 nM phalloidin-stabilized C167 F-actin seeds. The reaction was carried out in buffer A (as described for Figure 3). The inset is an EM image of the resulting C167PM bundles. (B) Polymerization of C167PM (15 μM, 100% labeled) in the presence of 3.0 mM $MgCl_2$ by an equimolar amount of phalloidin. The reaction was carried out in buffer A. The inset is an EM image of the resulting actin bundles.

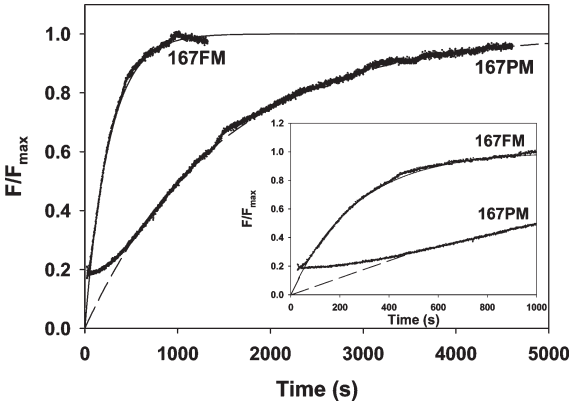

FIGURE 5: Polymerization kinetics of C167PM (12 μM, 69% labeled) and C167 actin labeled with fluoresceine maleimide (C167FM, 12 μM, 69% labeled). All reactions were carried out in buffer A. Actin polymerization was induced by 3.0 mM $MgCl_2$. F_{max} values were determined from the best data fits (C167FM, solid line; C167PM, dashed line) using SigmaPlot version 9. A lag phase was observed during the initial phase of C167PM actin polymerization (inset).

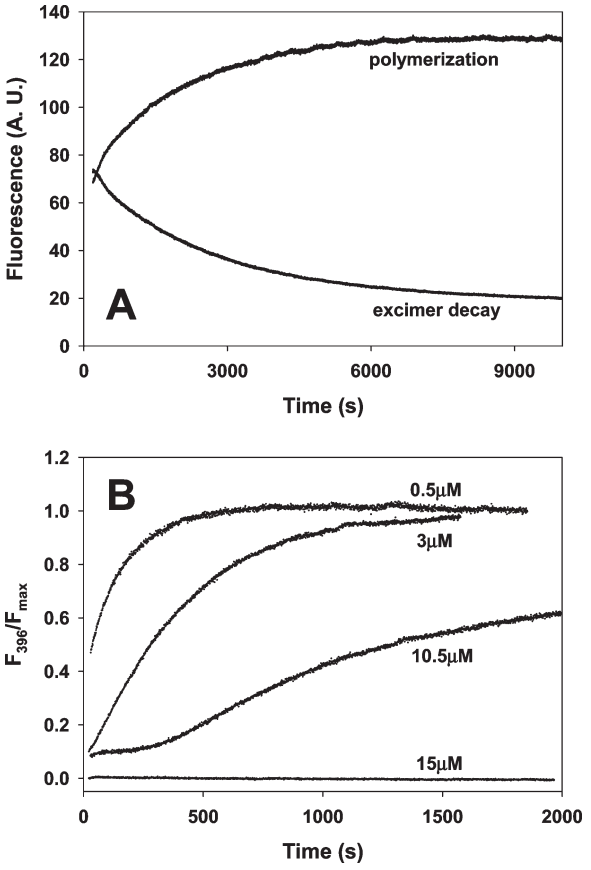

FIGURE 6: (A) Representative curves of C167PM polymerization (top trace) and pyrene excimer decay (bottom trace). Excitation at 344 nm and emission at 396 and 455 nm. Conditions: buffer A at 25 °C. (B) Rates of elongation decrease with increasing amounts of C167PM in the polymerization reaction mixtures. Unlabeled C167 mutant and the C167 actin labeled with pyrene maleimide (C167PM) were premixed at different ratios with a total actin concentration of 15 μM. Polymerization reactions were initiated with the addition of 3.0 mM $MgCl_2$. The concentration of C167PM in each mixture is shown next to the curves. Experimental conditions: buffer A at 20 °C.

pyrene excimer decay (λ = 455 nm). A representative plot of these data is shown in Figure 6A. This and similar comparisons of filament elongation rates and the rates of excimer decay at different C167PM actin concentrations revealed that the former were always faster than the latter. These data indicate that the APD is incorporated into filaments, and then either the APD transforms into other species, with a geometry incompatible with the pyrene excimer, or one of the two APD protomers "falls off" after the incorporation. Clearly, increasing the mole ratio of C167PM to the unlabeled C167 actin in a polymerization reaction mixture decreases the rate of filament elongation (Figure 6B). Thus, the APD also appears to inhibit the elongation of actin filaments.

The results presented above are in good agreement with those obtained for the polymerization of pyrene-labeled skeletal actin by polylysine (Figure 1D). Actin filament elongation data shown in Figure 1D could be fitted to a single-exponential equation with a rate constant of 0.054 s^{-1}, while the excimer decay (in the same plot) had a fast and slow phase that could be fitted with two rate constants, 0.037 and 0.0005 s^{-1}. Thus, as with the C167PM yeast actin, the rate of α-actin filament elongation is faster than the rate of the initial (fast phase) excimer decay and points to the incorporation of the APD into filaments in the polylysine-induced actin polymerization.

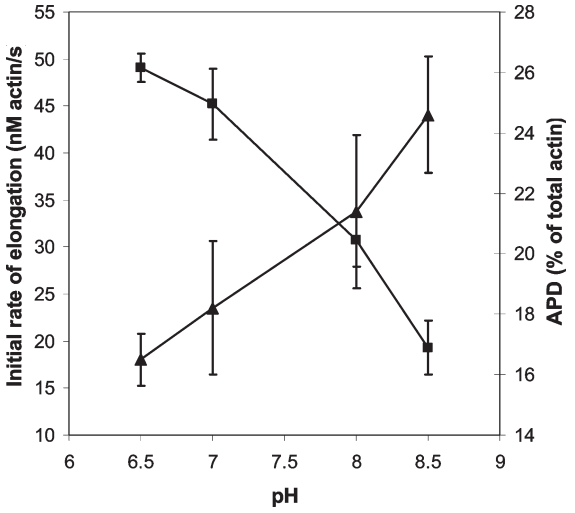

FIGURE 7: Effect of pH on the APD formation and on initial rates of actin (2.0 μM) polymerization with the addition of 4.0 μM polylysine. For elongation (■), polylysine was added to MgATP-G-actin (15% pyrene maleimide-labeled) and the fluorescence increase was followed with time. For APD formation (▲), polylysine was added immediately after the addition of 3.0 μM MTS-1 to actin which was followed after 30 s by 1.0 mM NEM to quench the cross-linking reaction. Reaction products were analyzed by SDS−PAGE. Error bars correspond to mean errors from three independent experiments.

To shed light on the relationship between the initial elongation rate of filaments and the formation of the APD, we examined the pH dependence of these two processes on samples containing 4.0 μM polylysine, 0.2 mM $MgCl_2$, and 2.0 μM MgATP-G-actin. The relative amounts of the APD in these samples were assessed using the MTS-1 cross-linking method described above. As shown in Figure 7, the initial rates of elongation decreased while the amount of APD increased with an increase in pH, confirming again the inverse correlation between APD formation and filament elongation.

The APD Persists in Actin Bundles. It was suggested previously that the APD might play a role in the bundling (*24*) and/or branching (*2*) of actin filaments. As shown in Figure 8A (inset), polylysine-induced actin polymerization leads to extensive bundle formation. According to the EM images, most of the filaments form tight bundles shortly after the initiation (30 s) of polylysine-induced polymerization. We used MTS-1 cross-linking to test for the presence (if any) of the APD in such bundles. Specifically, we increased the time interval between the addition of polylysine and MTS-1 to MgATP-G-actin and monitored the amount of the cross-linked APD in the bundles (Figure 8A). For time zero, MTS-1 was added immediately before polylysine; for all other time intervals, polylysine was added first, followed by MTS-1 (Figure 8A). The highest yield of the APD was observed when MTS-1 was added first; the yield diminished sharply when the order of addition was reversed, even when the delay between polylysine and MTS-1 addition was only 30 s. Notably, already 30 s after polylysine addition, actin filaments were bundled extensively in the absence of MTS-1, without any major disordering of the filaments (Figure 8A, inset). However, it should be noted that even 2 h after the onset of polymerization a significant amount of the APD was still detected by MTS-1 cross-linking.

To clarify the nature of the "persistent APD dimer" and how it is related to the polymerization and bundling, we used "mature" actin filaments prepolymerized with 2.0 mM $MgCl_2$. As expected,

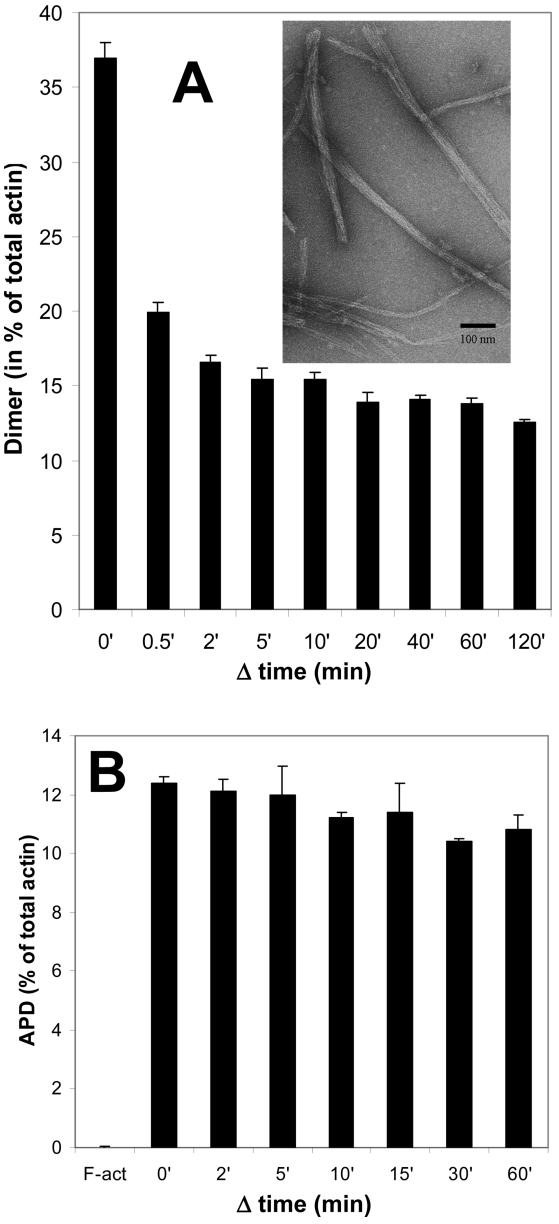

FIGURE 8: Dependence of ADP dimer formation on the time interval (Δtime) between additions of polylysine and MTS-1 to actin. After incubation with MTS-1 for 1.0 min, 1.0 mM NEM was added to stop the cross-linking reaction and the products were analyzed by SDS−PAGE. Error bars correspond to mean errors from three independent experiments. (A) Reactions were started with the addition of 8.0 μM polylysine and 0.2 mM $MgCl_2$ to 3.0 μM MgATP-G-actin in G buffer. This was followed by the addition of 2.0 μM MTS-1 after the indicated time interval, except for time zero, when MTS-1 was added first, followed immediately by the polylysine and $MgCl_2$. The inset is an EM image of 3.0 μM Mg-F-actin 30 s after the addition of 8.0 μM polylysine and 0.2 mM $MgCl_2$ (MTS-1 is absent) showing bundled actin filaments. (B) In all cases, except for "F-act", 8.0 μM polylysine and 0.2 mM $MgCl_2$ were added to 4.0 μM Mg-F-actin (prepolymerized for 60 min with 2.0 mM $MgCl_2$ in a low-ionic strength buffer), followed by the addition of 3.0 μM MTS-1 after the indicated time interval. In F-act, only MTS-1 was added.

after maturation of actin filaments, no cross-linking by MTS-1 was detected in the absence of polycations (Figure 8B). However, the cross-linked APD was observed after the Mg-polymerized F-actin was bundled by polylysine (Figure 8B). In this case, the dimer was produced at reduced levels, equivalent to the long time intervals in Figure 8A. Notably, there was little change, if any, in the amount of the cross-linked dimer with a delay time between polylysine and MTS-1 additions. Similar results were obtained upon bundling of mature actin filaments by lysozyme or spermine (data not shown). Taken together, these results show that the APD concentration decreases with the polymerization and bundling of actin, leveling off at ~10−15% of the total actin concentration. Most likely, this persistent presence of the APD is due to an antiparallel arrangement of actin filaments in the bundles.

The question of whether the transient presence of the APD in the filaments facilitates the formation of bundles by seeding the growth of antiparallel aligned filaments remains open (*24*). Notably, in this context, C167PM actin (containing the APD) but not C167FM actin (without the APD) forms bundles upon its copolymerization with unlabeled actin or its polymerization in the presence of phalloidin (data not shown).

DISCUSSION

Novel Tools for Studying the APD. Polylysine has been used as a model compound to study polycation-induced actin polymerization and the role of APD in this process (*4*). Here we characterized this reaction quantitatively using stopped-flow and fluorescence spectroscopy methods. Under the conditions of our experiments, the formation of the APD appears to be completed within ~0.2 s of polylysine addition and its level starts decreasing 8−9 s into the polymerization reaction. Assessment of relative amounts of the APD formed in this reaction requires fast and efficient cross-linking reagents. The conventional approach has been to monitor the formation of the APD via its pPDM cross-linking, which occurs at pH 9.2 while the polymerization of actin is conducted at a lower pH (*1*, *3*). The MTS cross-linking used in this study allows for dimer detection at the pH of the polymerization reaction, and it is sufficiently fast and effective to limit the reaction to 30 s [notably, MTS-1 appears to cross-link more efficiently than pPDM under identical experimental conditions (Figure 2)].

Although the above-mentioned cross-linking method enables comparative measurements of the presence of dimer under various conditions, it does not yield an equilibrium concentration of dimers for two reasons. First, the polymerization that proceeds during the cross-linking removes some monomers from the actin pool and shifts the monomer−APD equilibrium. Second, the cumulative nature of the cross-linking approach may also shift the monomer−APD equilibrium, albeit in the opposite direction. Thus, in this study we introduce a novel tool for probing the APD, a pyrene-labeled yeast actin mutant C167 (C167PM). Dimer formation in this case is pyrene-driven and occurs because of hydrophobic interactions between pyrene molecules attached to the reactive C167 on actin. No dimers were observed in the unlabeled samples of C167 actin or when this mutant was labeled with acrylodan or fluoresceine maleimide. C167PM yields sufficient amounts of a stable APD in solution to allow for kinetic measurements of its transformation and decay upon actin polymerization (Figures 3A and 6A). Although the dynamic properties of such dimer may be different from those of the unmodified APD, the advantage of this system is that neither chemical cross-linking nor polymerization-affecting compounds (polycations) are needed to obtain the C167PM antiparallel dimer. This new system opens the way for assessing the effect of the APD on actin polymerization under physiological conditions (pH, ionic strength, and Mg^{2+} concentration) and for testing conformational transitions in the APD during nucleation−polymerization reactions. The K_d of the C167PM dimerization

(0.34 μM) suggests a tight protomer−protomer interaction (Figure 3B) and allows for easy assessment of the APD concentration in solution. This system is designed mostly for in vitro studies, in which it may be used to investigate the role of the APD in polymerization assisted by actin-binding proteins.

The APD Inhibits Actin Nucleation. Bubb et al. (*4*) proposed a mechanism for actin nucleation through a conformational reorganization of the APD in nuclei driven by interactions (between two such dimers) similar to those observed in a crystal structure. However, no experimental evidence for this hypothesis was provided since the APD formed in the presence of latrunculin and polylysine could not polymerize. To test the hypothesis, Galinska-Rakoczy et al. (*3*) used EM analysis and pPDM cross-linking and explored the initial stages of actin polymerization by a monovalent salt. These authors linked the APD to the initial disordering of actin filaments rather than to their nucleation. However, because of limitations of the pPDM cross-linking and the lack of a pyrene excimer signal in their system, the connection between the observed filament disorder and the presence of the APD was not established conclusively (*3*). C167PM mutant actin appears to be a suitable system for testing the role of APD in actin polymerization. The results of our experiments lead to the following conclusions. (i) No actin trimers, tetramers, or higher-order protein species (i.e., potential nuclei) were detected in solutions of C167PM actin according to sedimentation equilibrium experiments (Figure 3B). (ii) C167PM mutant actin (100% labeled with pyrene maleimide) did not nucleate filament formation and inhibited the polymerization of the unlabeled C167 actin (Figure 4). (iii) In the case of α-actin, the inverse pH dependence of actin polymerization rates and the amounts of the APD (by MTS-1 cross-linking) also argue against the participation of APD in actin nucleation.

Incorporation of the APD into the Growing Filaments. A comparison of the rates of actin elongation and pyrene excimer decay revealed that in both polymer systems (α-actin with polycations and C167PM actin) the disappearance of the APD proceeds at a rate slower than the rate of filament elongation. This suggests incorporation of the APD into growing filaments and is inconsistent with dimer dissociation due to the shifting G-actin−F-actin equilibrium and/or its disappearance because of transformation into the nuclei of filaments. Moreover, the results obtained with C167PM actin show that the APD inhibits actin filament elongation. The fact that elongation rates decrease in the mixture of C167 and C167PM actin with an increasing fraction of the latter (and thus the APD) leads to the conclusion that the APD can be trapped transiently in the filaments, inhibiting their elongation, with a subsequent rearrangement or loss of the clashing antiparallel actin protomer. This is consistent with the scenario suggested by Steinmetz et al. for the disappearance of the APD from mature filaments (*2*).

A novel observation of this study is the finding of a relatively persistent population of dimers (10−15% of total actin) in actin bundles induced by polycations (Figure 8). Such a persistent presence of the APD has not been detected in a conventional polymerization of actin, but was captured by pPDM cross-linker (*1*) or MTS-1 (our unpublished results) in paracrystalline arrays of actin (polymerized by 50 mM $MgCl_2$). Since virtually all of the actin is bundled rapidly by polylysine (Figure 8A, inset), we attribute this persistent low amount of (cross-linked) dimers to the arrangement of filaments in the bundles. This arrangement could reflect either the previously proposed antiparallel packing of some filaments in the bundle (*24*−*26*) or, less likely, an occasional juxtaposition of Cys374 residues on parallel filaments of α-actin. The fact that a similar stable population of cross-linked APD was observed also in bundles produced by polylysine from prepolymerized and mature filaments (Figures 8B), which did not have antiparallel dimers before their bundling, provides evidence of the presence of oppositely oriented filaments in the bundles.

In line with this, our experiments showing C167 actin bundling upon its mixing and copolymerization with C167PM (containing the APD) suggest a possible role of the APD, relevant to a number of cellular processes, in facilitating the formation of bundles by seeding the growth of antiparallel oriented filaments. Together with the previously observed actin filament branching in preparations containing cross-linked APD (*2*), these results raise the possibility that the APD may be utilized in vivo by the filament branch stabilizing (such as cortactin) (*27*) and gelsolin family proteins (*28*).

ACKNOWLEDGMENT

We are grateful to Sergey Ryazantsev and Zeynep A. Oztug Durer for the technical assistance with EM. We thank Dr. Peter Rubenstein and Melissa McKane (University of Iowa, Iowa City, IA) for the yeast strain expressing the A167C/C374A (C167) actin mutant.

SUPPORTING INFORMATION AVAILABLE

Crystal structure of the APD (PDB entry 1LCU) (*4*) showing the Cα−Cα distance between the residues at position 167 in the dimer (Figure S1). This material is available free of charge via the Internet at http://pubs.acs.org.

REFERENCES

1. Millonig, R., Salvo, H., and Aebi, U. (1988) Probing actin polymerization by intermolecular cross-linking. *J. Cell Biol. 106*, 785–796.
2. Steinmetz, M. O., Goldie, K. N., and Aebi, U. (1997) A correlative analysis of actin filament assembly, structure, and dynamics. *J. Cell Biol. 138*, 559–574.
3. Galinska-Rakoczy, A., Wawro, B., and Strzelecka-Golaszewska, H. (2009) New aspects of the spontaneous polymerization of actin in the presence of salts. *J. Mol. Biol. 387*, 869–882.
4. Bubb, M. R., Govindasamy, L., Yarmola, E. G., Vorobiev, S. M., Almo, S. C., Somasundaram, T., Chapman, M. S., Agbandje-McKenna, M., and McKenna, R. (2002) Polylysine induces an antiparallel actin dimer that nucleates filament assembly. *J. Biol. Chem. 277*, 20999–21006.
5. Brown, S. S., and Spudich, J. A. (1979) Nucleation of polar actin filament assembly by a positively charged surface. *J. Cell Biol. 80*, 499–504.
6. Oriol-Audit, C. (1978) Polyamine-induced actin polymerization. *Eur. J. Biochem. 87*, 371–376.
7. Grant, N. J., Oriol-Audit, C., and Dickens, M. J. (1983) Supramolecular forms of actin induced by polyamines: An electron microscopic study. *Eur. J. Cell Biol. 30*, 67–73.
8. Brooks, W. H. (1995) Polyamine involvement in the cell cycle, apoptosis, and autoimmunity. *Med. Hypotheses 44*, 331–338.
9. Pignatti, C., Tantini, B., Stefanelli, C., and Flamigni, F. (2004) Signal transduction pathways linking polyamines to apoptosis. *Amino Acids 27*, 359–365.
10. Boggs, J. (2006) Myelin basic protein: A multifunctional protein. *Cell. Mol. Life Sci. 63*, 1945–1961.
11. Tang, J. X., Szymanski, P. T., Janmey, P. A., and Tao, T. (1997) Electrostatic effects of smooth muscle calponin on actin assembly. *Eur. J. Biochem. 247*, 432–440.
12. Beall, B., and Chalovich, J. M. (2001) Fesselin, a synaptopodin-like protein, stimulates actin nucleation and polymerization. *Biochemistry 40*, 14252–14259.
13. Tang, J. X., Ito, T., Tao, T., Traub, P., and Janmey, P. A. (1997) Opposite effects of electrostatics and steric exclusion on bundle

formation by F-actin and other filamentous polyelectrolytes. *Biochemistry 36*, 12600–12607.
14. Yarmola, E. G., Edison, A. S., Lenox, R. H., and Bubb, M. R. (2001) Actin filament cross-linking by MARCKS. *J. Biol. Chem. 276*, 22351–22358.
15. Spudich, J. A., and Watt, S. (1971) The regulation of rabbit skeletal muscle contraction. *J. Biol. Chem. 246*, 4866–4871.
16. Grintsevich, E. E., Benchaar, S. A., Warshaviak, D., Boontheung, P., Halgand, F., Whitelegge, J. P., Faull, K. F., Ogorzalek Loo, R. R., Sept, D., Loo, J. A., and Reisler, E. (2008) Mapping the cofilin binding site on yeast G-actin by chemical cross-linking. *J. Mol. Biol. 377*, 395–409.
17. Kouyama, T., and Mihashi, K. (1981) Fluorimetry study of N-(1-pyrenyl)iodoacetamide-labelled F-actin. *Eur. J. Biochem. 114*, 33–38.
18. Bradford, M. M. (1976) A rapid and sensitive method for the quantitation of microgram quantities of protein utilizing the principle of protein-dye binding. *Anal. Biochem. 72*, 248–254.
19. Kuang, B., and Rubenstein, P. A. (1997) Beryllium fluoride and phalloidin restore polymerizability of a mutant yeast actin (V266G, L267G) with severely decreased hydrophobicity in a subdomain 3/4 loop. *J. Biol. Chem. 272*, 1237–1247.
20. Cohn, E. J., and Edsall, J. T. (1943) Density and Apparent Specific Volume of Proteins. In Proteins, Amino Acids and Peptides as Ions and Dipolar Ions (Cohn, E. J., and Edsall, J. T., Eds.) pp 370−381, Reinhold Publishing Corp., New York.
21. Laue, T. M., Shah, B. D., Ridgeway, T. M., and Pelletier, S. L. (1992) Computer-Aided Interpretation of Analytical Sedimentation Data for Proteins. In Analytical ultracentrifugation in biochemistry and polymer science (Harding, S. E., Rowe, A. J., and Horton, J. C., Eds.) pp 90−125, The Royal Society of Chemistry, Cambridge, U.K.
22. Lehrer, S. S. (1997) Intramolecular Pyrene Excimer Fluorescence: A Probe of Proximity and Protein Conformational Change. In Methods in Enzymology: Fluorescence Spectroscopy (Brand, L., and Johnson, M. L., Eds.) pp 286−295, Academic Press, San Diego.
23. Shewmaker, F., Wickner, R. B., and Tycko, R. (2006) Amyloid of the prion domain of Sup35p has an in-register parallel β-sheet structure. *Proc. Natl. Acad. Sci. U.S.A. 103*, 19754–19759.
24. Pederson, T., and Aebi, U. (2003) Actin in the nucleus: What form and what for? *J. Struct. Biol. 140*, 3–9.
25. Francis, N. R., and DeRosier, D. J. (1990) A polymorphism peculiar to bipolar actin bundles. *Biophys. J. 58*, 771–776.
26. Steinmetz, M. O., Hoenger, A., Tittmann, P., Fuchs, K. H., Gross, H., and Aebi, U. (1998) An atomic model of crystalline actin tubes: Combining electron microscopy with X-ray crystallography. *J. Mol. Biol. 278*, 703–711.
27. Olazabal, I. M., and Machesky, L. M. (2001) Abp1p and cortactin, new "hand-holds" for actin. *J. Cell Biol. 154*, 679–682.
28. Hesterkamp, T., Weeds, A. G., and Mannherz, H. G. (1993) The actin monomers in the ternary gelsolin:2 actin complex are in an antiparallel orientation. *Eur. J. Biochem. 218*, 507–513.